Geophysical Research Letters

RESEARCH LETTER
10.1029/2023GL105042

Origins of Uncertainty in the Response of the Summer North Pacific Subtropical High to CO_2 Forcing

Kezhou Lu[1], **Jie He**[1], **and Isla R. Simpson**[2]

[1]School of Earth and Atmospheric Sciences, Georgia Institute of Technology, Atlanta, GA, USA, [2]National Center for Atmospheric Research, Boulder, CO, USA

Key Points:

- Model spread in the response of the summer North Pacific Subtropical High (NPSH) to CO_2 stems from model spread in simulating tropical processes
- Model spread in tropical sea surface temperature (SST) changes modulates the NPSH by influencing tropical precipitation
- Model spread in tropical precipitation changes independent of model spread in SST changes also adds to the uncertainty of the NPSH response

Supporting Information:

Supporting Information may be found in the online version of this article.

Correspondence to:

K. Lu,
kezhou.lu@eas.gatech.edu

Citation:

Lu, K., He, J., & Simpson, I. R. (2023). Origins of uncertainty in the response of the summer north Pacific subtropical high to CO_2 forcing. *Geophysical Research Letters*, *50*, e2023GL105042. https://doi.org/10.1029/2023GL105042

Received 16 JUN 2023
Accepted 28 OCT 2023

Author Contributions:

Conceptualization: Kezhou Lu
Data curation: Kezhou Lu
Formal analysis: Kezhou Lu
Funding acquisition: Jie He
Investigation: Kezhou Lu, Jie He, Isla R. Simpson
Methodology: Kezhou Lu, Jie He, Isla R. Simpson
Project Administration: Jie He
Resources: Jie He, Isla R. Simpson
Software: Kezhou Lu, Isla R. Simpson
Supervision: Jie He, Isla R. Simpson

Abstract The variability of the summer North Pacific Subtropical High (NPSH) has substantial socioeconomic impacts. However, state-of-the-art climate models significantly disagree on the response of the NPSH to anthropogenic warming. Inter-model spread in NPSH projections originates from models' inconsistency in simulating tropical precipitation changes. This inconsistency in precipitation changes is partly due to inter-model spread in tropical sea surface temperature (SST) changes, but it can also occur independently of uncertainty in SST changes. Here, we show that both types of precipitation uncertainty influence the NPSH via the Matsuno-Gill wave response, but their relative impact varies by region. Through the modulation of low cloud fraction, inter-model spread of the NPSH can have a further impact on extra-tropical land surface temperature. The teleconnection between tropical precipitation and the NPSH is examined through a series of numerical experiments.

Plain Language Summary The North Pacific Subtropical High (NPSH) is a semi-permanent high-pressure system located in the subtropical North Pacific. The variability in the summer NPSH has a significant impact on the monsoon and typhoons over East Asia and the hydroclimate of California. However, future projections of the NPSH using state-of-the-art climate models remain highly uncertain. By evaluating how much individual models deviate from the multi-model mean at different locations, we find four hot spots of high uncertainty in NPSH projections. Our analysis further reveals that the primary source of model variance in changes in the NPSH is tropical precipitation, which can be attributed to both inter-model SST-driven and non-inter-model SST-driven factors. Through numerical experiments, we demonstrate that the teleconnection between tropical precipitation and the NPSH is achieved through wave propagation.

1. Introduction

The North Pacific Subtropical High (NPSH) plays a crucial role in shaping the hydroclimate in the North Pacific, East Asia and North America. As part of the subtropical stationary wave system, the NPSH reaches its peak magnitude in the boreal summer ranging from 15°N to 45°N with its western branch extending to East Asia and eastern branch bordering North America (Wills et al., 2019). The western flank of the NPSH (WNPSH) transports moisture from the ocean to East Asia and the Indochina Peninsula, strengthening the Meiyu-Baiu rainfall and causing typhoons and floods (B. Wang et al., 2013; S. Zhou et al., 2019; Y. Wang et al., 2022). Meanwhile, the west coast of North America experiences warm and dry summers under the influence of the eastern flank of the NPSH (Burls et al., 2017; Seager et al., 2019). The response of the NPSH to anthropogenic warming is expected to significantly impact regional climates (Wills et al., 2019; Seager et al., 2019; J. Choi et al., 2016; W. Choi & Kim, 2019); therefore, reliable future projections of the NPSH are crucial for preparing adaptation and mitigation plans.

State-of-the-art climate models participating in the fifth and sixth phases of the Coupled Model Intercomparison Project (CMIP5 and CMIP6) exhibit diverging responses of the summer NPSH under global warming (Li et al., 2012; Sigmond et al., 2007; C. He & Zhou, 2015; X. Chen et al., 2020; D. Huang et al., 2022; Park & Lee, 2021). The explanations for models' poor agreement on the summer NPSH projections can be broadly categorized into local and remote processes. Local contributors include subtropical land-sea moist static energy (MSE) contrast and subtropical sea surface temperature (SST) (Lindzen & Nigam, 1987). For example, Shaw and Voigt (2015) and Baker et al. (2019) proposed that the opposing effects of CO_2 induced land-sea MSE contrast and subtropical SST warming result in a weak and insignificant NPSH response. In addition, model differences in the NPSH response are also attributed to the inter-model spread in the pattern of SST changes over the subtropical

Validation: Kezhou Lu, Jie He, Isla R. Simpson
Visualization: Kezhou Lu
Writing – original draft: Kezhou Lu
Writing – review & editing: Kezhou Lu, Jie He, Isla R. Simpson

oceans (P. Huang et al., 2013; Levine & Boos, 2019). Furthermore, previous studies have demonstrated that the model differences in simulating East Asian summer monsoons (Rodwell & Hoskins, 2001; S. Zhou et al., 2019), the surface sensible heating over the Tibetan Plateau (Duan et al., 2017), and subgrid-scale topography (Boos & Hurley, 2013) also impact the NPSH projections.

Of all the remote factors contributing to uncertainties in the projections of the NPSH, model differences in the response of tropical precipitation is suggested to play a significant role (Baker et al., 2019; X. Chen et al., 2020; M. Chen et al., 2019; Park & Lee, 2021). Based on stationary wave theory, the summer subtropical highs are maintained by tropical and continental monsoon heating (e.g., Gill (1980); Ting et al. (2001); Rodwell and Hoskins (2001)). Therefore, model uncertainties in tropical diabatic heating could potentially propagate into the NPSH region as planetary Rossby waves and interact with the NPSH. The inter-model spread of tropical precipitation is shown to be connected to the tropical SST through convection processes (Xie et al., 2010a). For example, X. Chen et al. (2020) demonstrated that the model uncertainty in projecting the WNPSH is linked to inter-model spread of tropical SST, which involves a negative shortwave-convection-SST feedback. Specifically, a positive SST anomaly in the equatorial Pacific amplifies local convection, causing an increase in convective clouds. Consequently, incoming shortwave radiation is attenuated, leading to a decrease in the initial SST warming and the local convection. The restrained convection subsequently diminishes the intensity and the westward extension of the WNPSH. However, it is challenging to disentangle the relative impact of the tropical SST and precipitation on the inter-model spread of the NPSH projections in a coupled atmosphere-ocean system, given the complexity of their relationship (e.g., Xie et al. (2010b); P. Huang et al. (2013); J. He et al. (2014)). As a result, how model variability in tropical precipitation, both driven by inter-model SST spread and otherwise, influences the NPSH remains largely unexplored. Furthermore, the impacts of diabatic heating on subtropical highs have been examined primarily through idealized baroclinic wave models with a simplified atmosphere (Duan et al., 2017; Park & Lee, 2021; Rodwell & Hoskins, 2001; Ting et al., 2001). Therefore, the potential influences of diabatic heating on other factors such as land surface temperature (TS), which could potentially modulate the NPSH, have yet to be explored.

In this study, we utilize output from the coupled and atmosphere-only simulations from the Coupled Model Intercomparison Project (CMIP and AMIP) to identify the leading modes of inter-model spread in summer NPSH projections. We further explore the mechanisms underlying such uncertainties by prescribing diabatic heating in a comprehensive atmospheric general circulation model (AGCM) and a simple baroclinic stationary wave model. The relative roles of model differences in tropical precipitation independent of tropical inter-model SST spread and tropical precipitation driven by tropical inter-model SST spread are explored in detail. The connection between the inter-model spread of the NPSH projections and inter-model spread of extra-tropical land TS projections is also discussed.

2. Data and Method

2.1. CMIP and AMIP Data

We use monthly mean data from fully coupled Abrupt4 × CO_2 and pre-industrial control simulations of 46 models (Table S1 in Supporting Information S1) from both CMIP5 and CMIP6 (O'Neill et al., 2016; Taylor et al., 2012). Only one ensemble member (r1i1p1 or r1i1p1f1) is selected from each model. All data are interpolated to horizontal grids with 1° × 1° spacing and 17 pressure levels. To investigate the inter-model uncertainties that are independent of inter-model differences in SST changes, we analyze 15 AMIP models (Table S1 in Supporting Information S1) from both CMIP5 and CMIP6. Three AMIP scenarios are considered: (a) AMIPControl, the control simulation forced by observational monthly mean SST and sea ice concentration; (b) AMIP4 × CO_2, same as AMIPControl but with CO_2 concentration quadrupled; (c) AMIPFuture, same as AMIPControl except adding the SST anomaly pattern taken from CMIP3 experiments at the time of CO_2 quadrupling but adjusted to achieve a global mean warming of 4K in SST (Webb et al., 2017). The response (Δ) is calculated as the difference between forced and control simulation. We take the last 30-year June to August mean (JJAm) from the 150-year Abrupt4 × CO_2, and 30-year JJAm from AMIPFuture and AMIP4 × CO_2 as equilibrium responses. For each coupled model under the Abrupt4 × CO_2 scenario, we first compute its equilibrium global mean SST (ΔSST_{gm}) response,and subsequently adjust the response of other variables by the ratio $\frac{4}{\Delta SST_{gm}}$, assuming that these variables respond proportionally to changes in global mean SST. The multi-model ensemble mean (MMM)

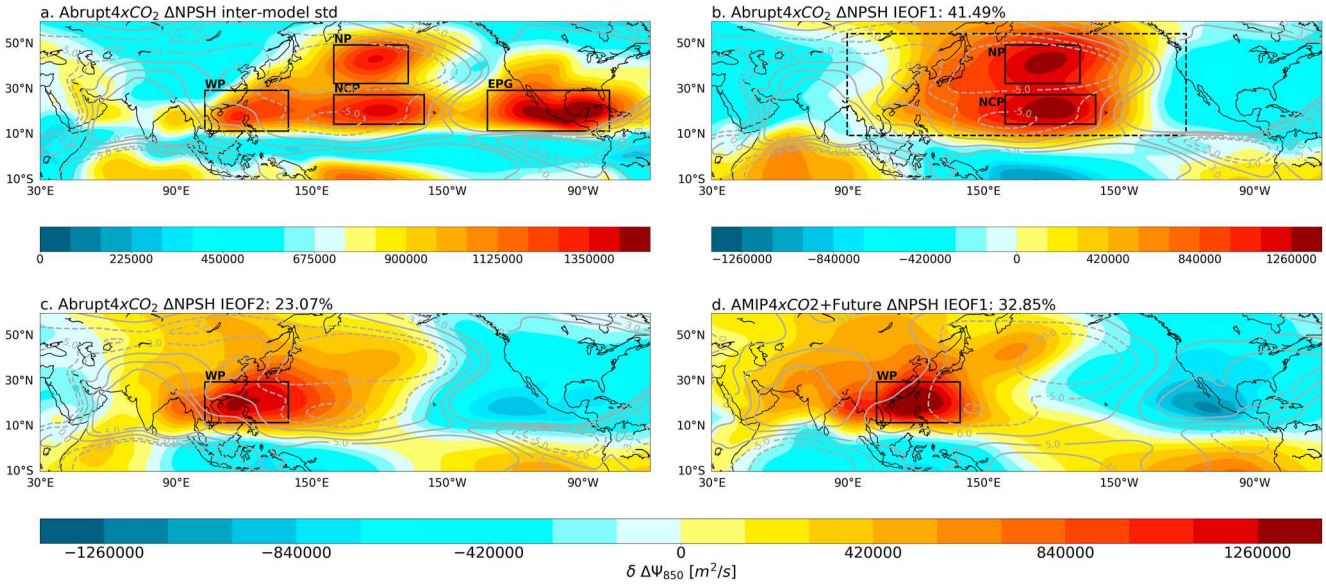

Figure 1. Inter-model spread of summer NPSH future projections. (a) The inter-model standard deviation of $\Delta\Psi_{850}$ under the Abrupt4 × CO_2 experiment. Four regions with high inter-model variability are marked with black rectangles. (b, c) The first two leading modes (IEOF1 and IEOF2) derived from IEOF analysis on $\Delta\Psi_{850}$ over the domain (10–50°N, 90–240°E; regions outlined with dashed line in (b) under Abrupt4 × CO_2 experiment. Panel (d) same as (b) but for AMIP4 × CO_2 + Future experiment. The gray contours denote the ΔNPSH MMM (unit: 10^6 m^2 s^{-1}) under Abrupt4 × CO_2 (a) to (c) and AMIP4 × CO_2 + Future (d), respectively. The percentage of inter-model variance explained by each mode is included in the subtitle.

equilibrium response of Abrupt4 × CO_2 is approximately equal to the summation of AMIP4 × CO_2 and AMIP-Future (AMIP4 × CO_2 + Future) (Figures S1 and S2 in Supporting Information S1; J. He and Soden (2015); Chadwick et al. (2017)).

We use eddy streamfunction at 850 hPa to represent the NPSH (Ψ_{850}) (Shaw & Voigt, 2015; Wills et al., 2019). Because diabatic heating is not a standard output from CMIP/AMIP, it was calculated as a residual from the time-mean thermodynamic energy equation (Rodwell & Hoskins, 2001):

$$\frac{\overline{Q}}{c_p} = \frac{\overline{\partial T}}{\partial t} + \left(\frac{p}{p_0}\right)^{\frac{R}{c_p}} \overline{\omega}\frac{\overline{\partial \theta}}{\partial p} + \overline{\mathbf{v}} \cdot \nabla_{\mathbf{p}}\overline{T} + \left(\frac{p}{p_0}\right)^{\frac{R}{c_p}} \frac{\partial}{\partial p}\overline{(\omega'\theta')} + \nabla_{\mathbf{p}} \cdot \overline{(\mathbf{v}'T')} \quad (1)$$

where Q is the diabatic heating or cooling, T is the temperature, c_p is the specific heat of dry air at constant pressure, R is the gas constant for dry air, p is the pressure, θ is the potential temperature, ω is the pressure velocity, and $\mathbf{v}$ are the horizontal wind velocities. The overbar represents the climatological June to August mean and prime is the deviation from that mean. Since monthly data is employed to calculate Equation 1, the resultant diabatic heating also includes the temperature tendency due to heat transport by sub-monthly transients. Over the tropical ocean, the pattern of vertically integrated diabatic heating resembles the pattern of precipitation as the diabatic heating is dominated by condensational heating (Hagos et al., 2010).

2.2. Inter-Model Uncertainty Analysis

We refer to the inter-model uncertainty (or spread) as the deviation of the equilibrium response of each individual model from the MMM (Figures S3 and S4 in Supporting Information S1). The regions with large inter-model spread were first identified via inter-model standard deviations (Figure 1a). The leading modes of inter-model variability are further analyzed by the rotated inter-model empirical orthogonal function with varimax criterion (IEOF) (Figures 1b–1d):

$$\delta\Delta X(m,s) = \sum_{i=1}^{n} IPC_{m,i} \cdot IEOF_{i,s} \quad (2)$$

where ΔX denotes the projected changes of variable X (e.g., Ψ_{850}, precipitation), δ is the deviation from the MMM, s is the number of spatial grid points, m is the number of models, and n is the number of modes. The principal

components (IPCs) are normalized. We opted for rotated IEOF over un-rotated IEOF to optimize the inter-model variance captured within the same modes, thus enhancing their physical interpretability.(Mestas-Nuñez, 2000). To quantify the connection between the spread in two variables (e.g., X and Y), we calculate the relationship between the inter-model variability in Y and the *i*th mode of IEOF of variable X, through two approaches: (a) by regressing *Y* onto the corresponding *i*th inter-model principal component (IPC_i) of *X*, or (b) by selecting where IPC_i values of *X* are statistically significant, that is, exceeding one standard deviation, and compositing *Y* using models with significant positive IPC_i values and models with significant negative IPC_i values.

With a limited number of models, the inter-model spread may be more sensitive to specific outliers. Therefore, we analyzed the inter-model standard deviations of ΔNPSH within a subset of 15 CMIP models for which the corresponding AMIP outputs are available (Figure S5a; Table S1 in Supporting Information S1). The similarity between Figure 1a and Figures S5a in Supporting Information S1 suggests that this subset of 15 models is sufficient to capture the spatial structures of ΔNPSH inter-model spread found in the larger ensemble.

2.3. Model Simulations

To investigate the physical mechanisms underlying the inter-model uncertainty of ΔNPSH, we use both the Community Atmosphere Model, version 5 (CAM5) within the framework of the Community Earth System Model, version 1 (CESM1) (Hurrell et al., 2013), and a baroclinic stationary wave model (SWmodel) (Held et al., 2002; Ting & Yu, 1998) to perform the sensitivity experiments. A comprehensive description of both models is provided in Table S2. Both CAM5 and the SWmodel are adequate for simulating the response of large-scale atmospheric circulation to prescribed forcing. However, CAM5 is more representative of the real atmosphere as it incorporates a much wider range of processes and is not subject to the relaxation toward a basic state or the idealized dampings that the SWmodel is. Specifically with CAM5, we are able to explore the associated response of land surface temperature, cloud cover and precipitation to prescribed forcing. In contrast, the SWmodel only focuses on the atmospheric stationary wave response which helps us to understand the dynamics and interactions of waves without confounding effects of other climate feedbacks. However, it is an idealized model in which interactions, such as eddy-feedbacks, must be prescribed, and it is kept stable through relaxation toward a specified basic state and the addition of idealized damping. The control simulation in CAM5 is forced with the climatological SSTs and sea ice concentrations taken from the pre-industrial simulation of the CESM1 Large Ensemble Project (LENS) (Kay et al., 2015). The basic state in the SWmodel is the three-dimensional boreal summer climatology including temperature and horizontal winds, derived from the same LENS pre-industrial simulation mentioned above. Note that the orography forcing is integrated into the 3D climatological basic state in SWmodel.

We explore the tropical influence on the NPSH via a series of diabatic heating sensitivity experiments. Specifically, we consider two types of inter-model spreads of the tropical diabatic heating ($\delta\Delta Q$): one that is independent of inter-model spread in tropical SST change ($\delta\Delta$SST) and the other that is induced by the tropical $\delta\Delta$SST. The $\delta\Delta$SST-independent $\delta\Delta Q$ is derived from the rotated IEOF analysis on AMIP4 × CO_2 + Future models over the entire tropics (30°S–30°N), where SST and changes in SST are the same among models. The pattern of vertically integrated diabatic heating resembles Figure 2c. To quantify $\delta\Delta Q$ attributed to tropical $\delta\Delta$SST, we begin by imposing the tropical $\delta\Delta$SST associated with $\delta\Delta NPSH$ on CAM5 control simulation. The SST anomalies are determined through the rotated IEOF analysis of the output from the CMIP Abrupt4 × CO_2 experiment ("Section 2.2," Figure 2d, and Figure S6 in Supporting Information S1). The resulting total diabatic heating anomaly (Figure S7a in Supporting Information S1) over the deep tropics (15°S–15°N) is then calculated as the sum of condensational heating, longwave heating, solar heating and vertical diffusion of temperature. The diabatic heating anomaly is added to the SWmodel as a constant temperature tendency term. For each SWmodel experiment, the model is integrated for 50 days, and the time average of the last 20 days is taken as the equilibrium response. Since CAM5 would non-linearly amplify the diabatic heating perturbation due to its moisture process and other feedbacks, we determine the diabatic heating perturbation to impose with an "iterative approach" as detailed in R. Chen et al. (2022). For each CAM5 experiment, five ensembles of three-month simulations are branched off on the first day of June of five different years. The equilibrium responses are calculated as the three-month mean of the differences between the forced and control runs averaged across all ensembles.

To compare the relative importance of inter-model spread in extra-tropical SST changes to the tropical influence, we prescribe the $\delta\Delta$SST associated with inter-model spread of ΔNPSH over the North Pacific (27–70°N) to CAM5. The North Pacific SST inter-model spread is calculated through inter-model composite analysis from Abrupt4 × CO_2 output ("Section 2.2," Figure S6 in Supporting Information S1).

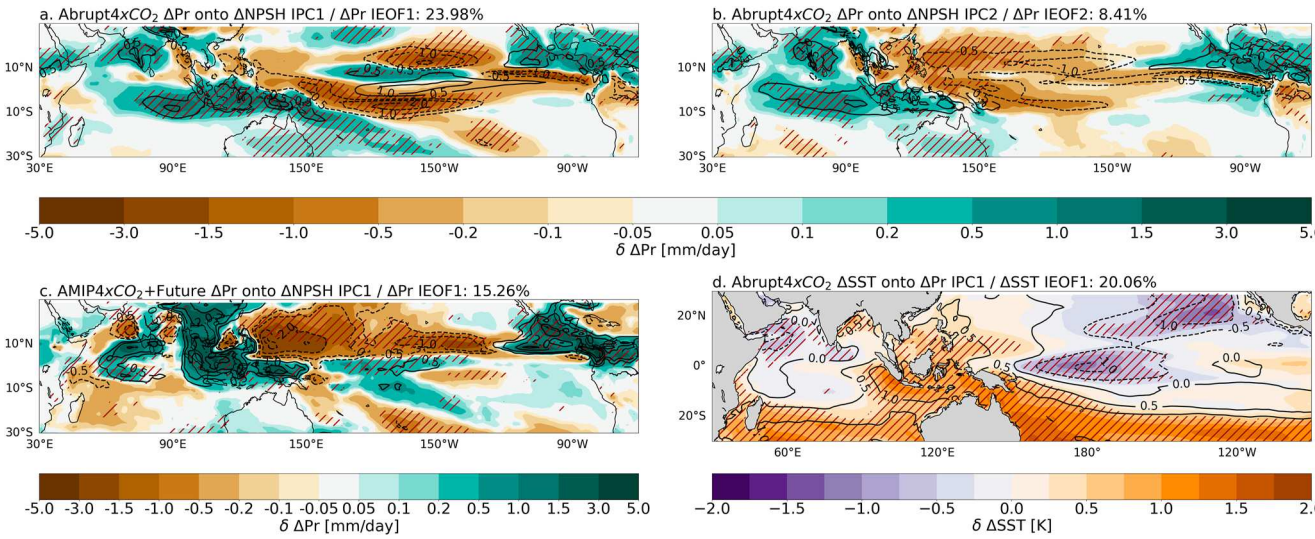

Figure 2. Tropical precipitation (Pr) and SST anomalies associated with ΔNPSH inter-model spread. (a) Tropical ΔPr regressed onto IPC1 of ΔNPSH (shadings) and IEOF1 of ΔPr (contours; mm/day) under Abrupt4 × CO_2 scenario. Panel (b) Similar to (a) but with ΔPr regressed onto IPC2 of ΔNPSH and IEOF2 of ΔPr. Panel (c) Similar to (a) and (b) but with ΔPr regressed onto IPC1 of ΔNPSH and IEOF1 of ΔPr under AMIP4 × CO_2 + Future. (d) Tropical ΔSST regressed onto IPC1 or ΔPr (shadings) and IEOF1 of ΔSST (contours; K). Regions with statistically significant correlations based on the Student's *t*-test are hatched.

3. Results

3.1. Overview of Inter-Model Spread in Summer NPSH Projection

The overall strength of summer NPSH weakens under the Abrupt4 × CO_2 scenario as indicated by the MMM response of Ψ_{850} (gray contours in Figure 1a) across 46 CMIP models. However, the inter-model standard deviation of ΔNPSH is comparable or even larger than the MMM response in most of the regions (comparing color shadings and contours in Figure 1a). We find four zones of high ΔNPSH inter-model variability: the western Pacific (WP), the eastern Pacific and Gulf of Mexico (EPG), the North Pacific (NP) and the central North Pacific (NCP). These four hot spots are well captured by the first two leading IEOF modes which account for nearly 65% of the inter-model variance (Figures 1b and 1c). Here we pick the sign of the eigenvectors that features a strengthening of the NPSH as the positive direction and all subsequent analyses follow this choice. The shape of the IEOF patterns, the amount of inter-model variance explained, and the underlying physical mechanisms remain the same regardless of our choice (Weare et al., 1976). The first IEOF features an overall strengthening of the NPSH with two centers of maximum variance located at the NP and the NCP respectively. The cyclones over the Asian continent and the EPG are also partially captured (Figure 1b). The second IEOF mode presents a dipole structure representing a strengthening and westward extension of the WNPSH, and a weakening of the NPSH over the eastern Pacific (Figure 1c). Mechanisms behind the two IEOF modes will be examined in the rest of the paper.

To exclude the influence from inter-model variability in SST changes, we evaluate the inter-model spread of the NPSH response among 15 models under AMIP4 × CO_2 + Future, where all models are driven by the same SST changes ("Section 2.1" and Table S1 in Supporting Information S1). Note that these 15 models are also included in the coupled Abrupt4 × CO_2 experiments and can capture the overall spatial patterns of ΔNPSH inter-model spread (Figure S8 in Supporting Information S1). As depicted in Figure S5b in Supporting Information S1, the WP region demonstrates a notable inter-model standard deviation among 15 AMIP4 × CO_2 + Future models. The leading inter-model variance pattern (Figure 1d) features a dipole structure with an anticyclone anomaly over the WP that resembles Figure 1c, suggesting that the inter-model spread of ΔWNPSH over the WP has causes not related to δΔSST. We've additionally examined the δΔSST associated with the IEOF2 of ΔNPSH under Abrupt4 × CO_2. As shown in Figure S9 in Supporting Information S1, the IPC2 of ΔNPSH does not significantly correlate to ΔSST in most of the regions (Figure S9b in Supporting Information S1). On the other hand, the high inter-model variances over the NP and NCP (Figure 1b) are either absent or underrepresented in Figure 1d and Figure S5b in Supporting Information S1, indicating that the inter-model uncertainties of ΔNPSH over the NP and the NCP might be related to ΔSST inter-model spread.

3.2. Tropical Origins of the Inter-Model Uncertainty

As a key driver of the tropical circulation and the tropical-extratropical teleconnections (Emanuel et al., 1994; Fereday et al., 2020; Gill, 1980), the tropical precipitation (Pr) remains one of the most challenging components in climate projections. We examined the inter-model variability in the equilibrium response of tropical precipitation under the Abrupt4 × CO_2 scenarios via the rotated IEOF method and evaluate their relationships with ΔNPSH. The IEOF1 of the tropical precipitation response displays a meridional alternating negative and positive anomaly structure spanning from the Indian Ocean to the subtropical Pacific (contours in Figure 2a). The second leading mode of the precipitation inter-model spread exhibits a southwest-northeast orientated dipole pattern with negative convection anomalies located in the west Pacific (contours in Figure 2b). The first two leading IEOF modes account for around 32% of the inter-model variance of the tropical precipitation response. When regressing the precipitation response onto the inter-model IPCs of ΔNPSH, we find the regression pattern associated with IEOF1 of ΔNPSH aligns closely with the corresponding IEOF1 of tropical ΔPr, while the regression pattern associated with IEOF2 of ΔNPSH aligns closely with the corresponding IEOF2 of tropical ΔPr (comparing shadings to contours in Figures 2a and 2b).

3.2.1. Contribution of $\delta\Delta$SST Independent Precipitation Uncertainty

Given the resemblance between Figures 1c and 1d, and the significant correlation between tropical precipitation and the NPSH, as suggested in Figure 2b, we initiated our investigation by focusing on non-$\delta\Delta$SST related precipitation inter-model spread. Under AMIP4 × CO_2 + Future (Figure 2c), the spatial pattern of IEOF1 of tropical precipitation response also exhibits a dipole pattern oriented from southwest to northeast over the Indo-West Pacific similar to Figure 2b. This precipitation dipole is related to an asymmetric diabatic heating with respect to the equator and this diabatic heating pattern will trigger a low-level anticyclone (cyclone) to the north (south) of the equator, as described by the Matsuno-Gill response (Gill, 1980; Matsuno, 1966). Indeed, the low-level anticyclone at the WP, and the cyclone at the Maritime Continent (MC) in Figures 1c and 1d appear to align with the Matsuno-Gill response to the Indo-West Pacific precipitation dipole anomalies demonstrated in Figures 2b and 2c. This consistency led us to hypothesize that the high $\delta\Delta$NPSH in the WP region can be triggered and sustained by $\delta\Delta$Q that is independent of tropical $\delta\Delta$SST.

To confirm our hypothesis, we conducted a set of sensitivity experiments in CAM5 and the SWmodel where the tropical (30°S–30°N) inter-model diabatic heating anomaly obtained from the AMIP4 × CO_2 + Future output is prescribed ("Section 2.3"). As demonstrated in Figures 3e and 3g, a quadrupole low-level circulation pattern with a strong anticyclone centered at the WP and a strong cyclone centered at the EPG appears as the primary response to the tropical diabatic heating. In the case of CAM5, the anomalous northeasterlies on the eastern flank of the anticyclone transport the off-equatorial dry (low moist enthalpy) air into the western Pacific, further suppressing the convection over the WP (Wu et al., 2017; Y. Wang et al., 2022). Moreover, the elevated land surface temperature over the extra-tropical Eurasian continent (Figure 4c) acts to reinforce the strengthening of the NPSH through the land-sea thermal contrast (Portal et al., 2022; Shaw & Voigt, 2015). The similar response of $\Delta\Psi_{850}$ between CAM5 (Figure 3e) and the SWmodel (Figure 3g) suggests that the strengthening of the NPSH over the WP can be primarily attributed to the Matsuno-Gill response triggered by tropical $\delta\Delta$Q. Besides the Matsuno-Gill response, the summer mean state of the Indo-West Pacific climate establishes a niche environment to sustain the low-level circulation anomalies over the WP region. This is achieved through the positive barotropic kinetic energy conversion from the climatological confluence between the monsoon westerlies and trade winds at low levels (Hoskins et al., 1983; X. Wang et al., 2021). The upper-level circulation presents a similar quadrupole pattern but with a cyclone over the western Pacific and anticyclone over North America and the EPG, suggesting a baroclinic wave structure between 15 and 20°N (Figures 3a and 3c) (Ting & Yu, 1998; Wills et al., 2019). As shown by the Takaya-Nakamura wave activity flux (Figure 3a), a northeastward propagating Rossby wave train emanates from the tropical western Pacific and extends to North America over the upper troposphere (Ding et al., 2018; Takaya & Nakamura, 1997). The upper-level eddy streamfunction response to non-$\delta\Delta$SST induced $\delta\Delta$Q, simulated by both CAM5 and the SWmodel, generally aligns with the statistical results derived from the IEOF analysis (Figures S10c and S10d in Supporting Information S1). In the SWmodel, the weaker response of barotropic structure above 40°N and the lack of low-level anticyclonic anomaly over the southwest of the Bering Sea, when compared to CAM5, could be attributed to the simplicity of the model and the absence of features such as anomalies in the transient eddies or extra-tropical diabatic processes (Figure S11 in Supporting Information S1), and non-linear interactions of the anomalies with topography.

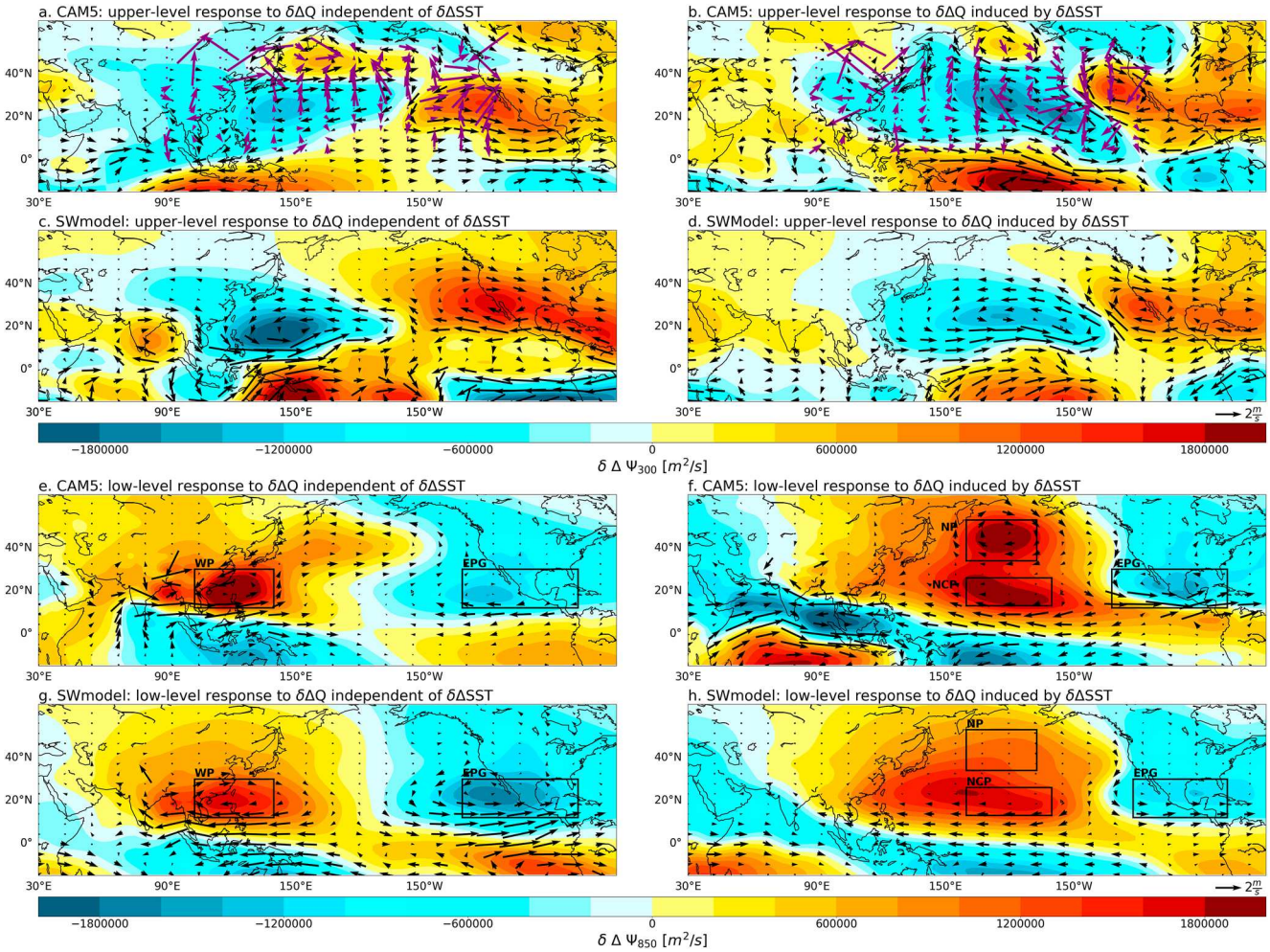

Figure 3. Response of subtropical circulation to prescribed tropical diabatic heating anomalies ($\delta\Delta Q$) in CAM5 and SWmodel. The left column shows the response of eddy streamfunction (shadings) and horizontal winds (black vectors; m/s) to $\delta\Delta Q$ independent of tropical ΔSST inter-model spread (δΔSST). The right column is similar to the left one but with the circulation response to tropical δΔSST induced $\delta\Delta Q$. Panels (a–d) describe the results at 300 hPa and (e–h) describe the results at 850 hPa. The stationary Rossby wave propagation is shown as the Takaya-Nakamura Flux (purple vectors; normalized) in (a) and (b). The CAM5 results are (a, b, e, and f) and the SWmodel results are (c, d, g and h).

3.2.2. Contribution of δΔSST-Driven Precipitation Uncertainty

The interaction between tropical SST and subtropical atmospheric circulation is often discussed in the context of the El Niño-Southern Oscillation teleconnection, such as the Pacific-North American pattern (e.g., Franzke et al. (2011); Dai et al. (2017)), Kelvin wave-induced Ekman divergence resulting from Indian Ocean (IO) warming (C. He & Zhou, 2014; Xie et al., 2009), local convection over a warm MC (Sui et al., 2007), moist enthalpy advection (Wu et al., 2017), and the ocean-atmosphere coupling between the IO SST and the Pacific-Japan pattern (Kosaka et al., 2013). In particular, by modifying the local convection, tropical SST can modulate the influence of tropical precipitation on atmospheric circulation via wave generation and propagation. Therefore, it is plausible to speculate that the inter-model spread of tropical SST affects the NPSH by generating anomalous tropical precipitation. The IEOF1 of tropical ΔSST features a La Niña-like pattern with cooling over the western Indian Ocean and central Pacific and a K-shaped warming anomaly covering the MC and the western subtropical Pacific (Figure 2d and Figure S9a in Supporting Information S1). This SST inter-model spread pattern is spatially correlated with the IEOF1 of precipitation (comparing contours to shadings in Figure 2d). In the meantime, the tropical precipitation anomaly regressed onto IPC1 of ΔNPSH (shadings in Figure 2a) perfectly lines up with the IEOF1 pattern of precipitation, implying that the high inter-model ΔNPSH variance at the NP and the NCP are connected to the tropical precipitation anomalies that are linked to the inter-model ΔSST uncertainty.

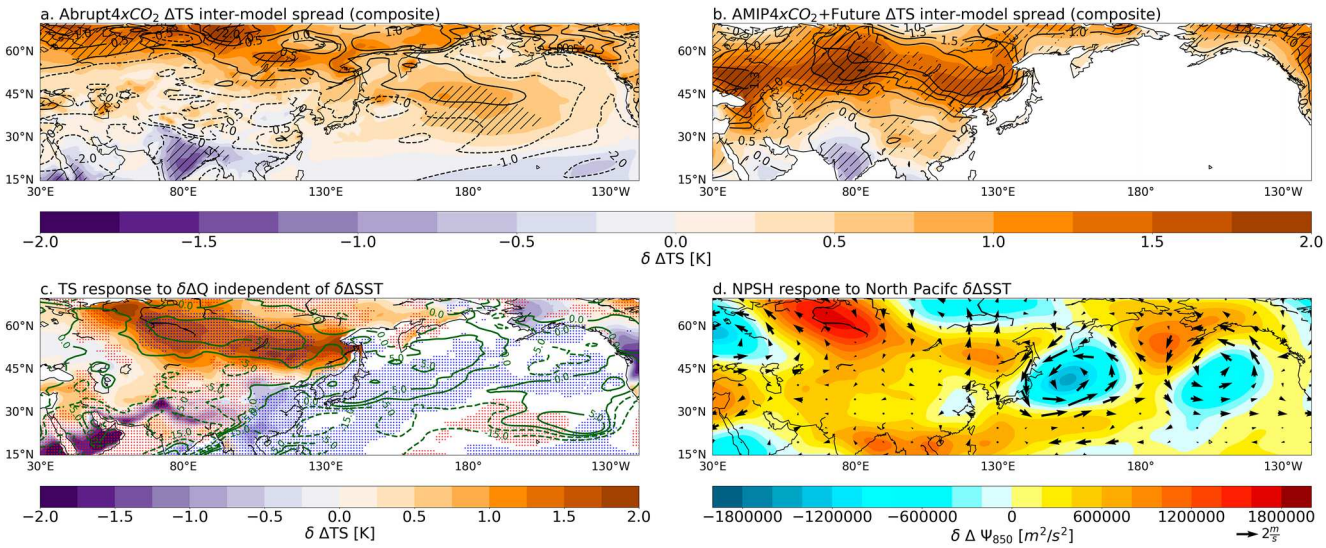

Figure 4. Relationship between inter-model uncertainty of ΔNPSH and extra-tropical land ΔTS and the North Pacific ΔSST. (a) Extra-tropical ΔTS regressed onto IPC2 of ΔNPSH (shadings) and inter-model uncertainty of ΔTS from composite analysis (contours; K). Panel (b) Similar to (a) but with land ΔTS regressed onto IPC1 of ΔNPSH and ΔTS inter-model uncertainty under the AMIP4 × CO_2 + Future. Regions with statistically significant correlations based on Students' *t*-tests are marked with hatches in (a) and (b). (c) Response of land TS (shadings; K), net surface shortwave radiation (thick green contours; W/m^2), and low cloud fraction (scatters in blue and red, where blue indicates a significant low cloud reduction and vice versa) to SST independent inter-model tropical diabatic heating spread in CAM5. (d) Response of NPSH (shadings) and horizontal winds (vectors; m/s) to North Pacific δΔSST.

The role of the tropical δΔSST-driven precipitation inter-model spread is further explored through numerical experiments ("Section 2.3"). To focus on the impact of inter-model precipitation uncertainty in the deep tropics, we only prescribe diabatic heating anomalies between 15°S and 15°N generated from the tropical δΔSST experiment to CAM5 and the SWmodel. As shown in both Figures 3f and 3h, a Matsuno-Gill type circulation response appears in the lower troposphere in both CAM5 and the SWmodel. However, the two high-pressure centers located at the NP and the NCP are only captured by CAM5. The IEOF1 pattern of ΔNPSH (Figure 1b) is well replicated in CAM5 except that the anomaly over the NCP is inclined toward the northwest. The NPSH response in the SWmodel displays only one high-pressure center located around NCP and this could result from neglecting other extra-tropical process such as transient eddy feedbacks (Figure S12 in Supporting Information S1). The circulation response in the upper troposphere in both CAM5 and the SWmodel exhibits a northeastward propagating Rossby wave train, a baroclinic wave structure between 15 and 20°N and a barotropic wave structure between 45 and 55°N (Figures 3b and 3d and Figure S10b in Supporting Information S1). It is worth mentioning that the influence of the tropical inter-model ΔSST spread extends beyond local convection to include precipitation changes in remote areas (contours in Figure S7b in Supporting Information S1). The secondary convection produced over the extra-tropics also exerts an impact on the NPSH along with the tropical convection. For instance, the positive precipitation anomaly over East China Sea triggers a local cyclonic circulation anomaly, restricting the westward extension of the δΔNPSH (shadings in Figure S7b in Supporting Information S1).

3.3. Relationship With the Extra-Tropics

While we have determined that the primary sources of model uncertainty in ΔNPSH are related to both δΔSST and non-δΔSST driven tropical precipitation inter-model spread, it is also important to consider the potential connections to extra-tropical SST and land TS. As illustrated in Figure 4a, the inter-model spread of land TS changes features an overall warming in northern Eurasia between 45 and 65°N and a cooling in South Asia and the Middle East. The high inter-model variability of ΔNPSH over the WP is statistically associated with this warming pattern over extra-tropical Eurasia, while the other three hot spots do not exhibit any significant correlations (shadings in Figure 4a, Figures S13 and S14 in Supporting Information S1). When examining the inter-model spread of extra-tropical land TS response under the AMIP4 × CO_2 + Future, we find a similar warming pattern between 45 and 65°N and this pattern is also significantly correlated with IPC1 of ΔNPSH (Figure 4b).

The conventional perspective believes that the strengthening of the NPSH is mostly driven by an enhanced land-sea thermal contrast (Levine & Boos, 2019; Li et al., 2012; Portal et al., 2022; Shaw & Voigt, 2015; Wills

et al., 2019). In addition to that, we find that a substantial portion of the inter-model spread of extra-tropical land warming over northern Eurasia (Figures 4a and 4b) can also be produced by prescribing CAM5 with non-$\delta\Delta$SST driven diabatic heating anomalies (shadings in Figure 4c). The westward extension of the anomalous low-level anticyclone induced by the tropical diabatic heating inter-model spread is evident over Eurasia (Figures 3e and 3g). This extension intensifies the subsidence of dry air and leads to a reduction in cloud fractions, particularly for low clouds (blue scatters in Figure 4c). The reduction of the low clouds further promotes the absorption of solar radiation by the land, leading to a net increase of the downwelling shortwave radiation at the land surface (thick green contours in Figure 4c). In addition, the anomalous low-level southerly winds contribute to the extra-tropical land warming by advecting warmer air from the tropics (Figures 3e and 3g). On the other hand, the extra-tropical Eurasian warming is also expected to reinforce the intensification of the $\delta\Delta$NPSH.

By regressing the inter-model ΔSST anomalies over the North Pacific onto the IPC2 of ΔNPSH, we find a warm anomaly stretching from the Kuroshio Extension to the west coast of Canada (Figure 4a). This warm SST anomaly along the Kuroshio Extension is also correlated with an enhancement of local precipitation and a reduction of precipitation to the north and south (Figure S15a in Supporting Information S1) (Gan & Wu, 2012). When prescribing the $\delta\Delta$SST over the North Pacific to CAM5 ("Section 2.3"), a very weak strengthening of the low-level circulation is seen over the NP, and two cyclonic circulations are shown in the western and eastern North Pacific as local responses to the enhancement of precipitation (Figure 4d and Figure S15b in Supporting Information S1). Nevertheless, the overall structure of the NPSH response is quite different from IEOFs of ΔNPSH (Figure 1). Conversely, the strengthening of the NPSH triggered by tropical precipitation inter-model spread leads to an overall reduction of low cloud fraction and intensification of downwelling surface shortwave radiation, which could partially explain the warming over the North Pacific (Figure 4c).

4. Summary and Discussion

We have confirmed that the model uncertainties in projections of the NPSH originate from both $\delta\Delta$SST and non-$\delta\Delta$SST driven tropical inter-model precipitation spread. Specifically, the large model variance of ΔNPSH over the WP is caused by inter-model precipitation uncertainty that is independent of $\delta\Delta$SST. This inter-model ΔNPSH spread further influences changes in extra-tropical Eurasian TS and the North Pacific SST through the modulation of low cloud fraction. On the other hand, the inter-model spread in the changes of tropical SST can affect the NPSH over the NP and the NCP through the production of anomalous precipitation.

Our study highlights the importance of accurately projecting the tropical precipitation. When the model variance is absent in ΔSST, the two plausible causes of inter-model precipitation spread could be models' diversity in cloud parameterization (Mauritsen & Stevens, 2015; Su et al., 2017) and tropical land albedo simulation (Levine & Boos, 2017; W. Zhou & Xie, 2017). In addition, other processes such as the subtropical transient eddy feedback (e.g., Hurrell et al. (2013)), the subtropical and mid-latitude cloud albedo feedback (Burls et al., 2017), and the Arctic amplification (e.g., Coumou et al. (2018)) might also contribute to the model uncertainty in projections of the NPSH and are worth deeper explorations.

Acknowledgments
We thank the two anonymous reviewers for their valuable and insightful comments. We also thank the computational resources provided by the Partnership for an Advanced Computing Environment (PACE) at Georgia Institute of Technology, and the Cheyenne supercomputer provided by the Computational and Information Systems Laboratory at the National Center for Atmospheric Research. KL and JH are supported by the National Science Foundation AGS-2047270. IRS is supported by the National Center for Atmospheric Research, which is a major facility sponsored by the National Science Foundation under the Cooperative Agreement 1852977.

Data Availability Statement

The CMIP5 data can be downloaded publicly at CMIP5 (2012) (or https://esgf-node.llnl.gov/projects/cmip5/), and the CMIP6 data can be downloaded publicly at CMIP6 (2016) (or https://esgf-node.llnl.gov/projects/cmip6/). The numerical experiment data of this paper are archived at Zenodo (Lu et al., 2023).

References

Baker, H. S., Woollings, T., Mbengue, C., Allen, M. R., O'Reilly, C. H., Shiogama, H., & Sparrow, S. (2019). Forced summer stationary waves: The opposing effects of direct radiative forcing and sea surface warming. *Climate Dynamics*, *53*(7), 4291–4309. https://doi.org/10.1007/s00382-019-04786-1

Boos, W. R., & Hurley, J. V. (2013). Thermodynamic bias in the multimodel mean boreal summer monsoon. *Journal of Climate*, *26*(7), 2279–2287. https://doi.org/10.1175/JCLI-D-12-00493.1

Burls, N. J., Muir, L., Vincent, E. M., & Fedorov, A. (2017). Extra-tropical origin of equatorial pacific cold bias in climate models with links to cloud albedo. *Climate Dynamics*, *49*(5), 2093–2113. https://doi.org/10.1007/s00382-016-3435-6

Chadwick, R., Douville, H., & Skinner, C. B. (2017). Timeslice experiments for understanding regional climate projections: Applications to the tropical hydrological cycle and European winter circulation. *Climate Dynamics*, *49*(9), 3011–3029. https://doi.org/10.1007/s00382-016-3488-6

Chen, M., Yu, J.-Y., Wang, X., & Jiang, W. (2019). The changing impact mechanisms of a diverse El Niño on the western pacific subtropical high. *Geophysical Research Letters*, *46*(2), 953–962. https://doi.org/10.1029/2018GL081131

Chen, R., Simpson, I. R., Deser, C., Wang, B., & Du, Y. (2022). Mechanisms behind the springtime north pacific ENSO teleconnection bias in climate models. *Journal of Climate*, *35*(23), 4091–4110. https://doi.org/10.1175/JCLI-D-22-0304.1

Chen, X., Zhou, T., Wu, P., Guo, Z., & Wang, M. (2020). Emergent constraints on future projections of the western north pacific subtropical high. *Nature Communications*, *11*(1), 2802. https://doi.org/10.1038/s41467-020-16631-9

Choi, J., Lu, J., Son, S.-W., Frierson, D. M. W., & Yoon, J.-H. (2016). Uncertainty in future projections of the north pacific subtropical high and its implication for California winter precipitation change. *Journal of Geophysical Research: Atmospheres*, *121*(2), 795–806. https://doi.org/10.1002/2015JD023858

Choi, W., & Kim, K.-Y. (2019). Summertime variability of the western north pacific subtropical high and its synoptic influences on the East Asian weather. *Scientific Reports*, *9*(1), 7865. https://doi.org/10.1038/s41598-019-44414-w

CMIP5. (2012). Coupled model intercomparison project 5 (CMIP5) [Dataset]. CMIP5. Retrieved from https://esgf-node.llnl.gov/projects/cmip5/

CMIP6. (2016). Coupled model intercomparison project 6 (CMIP6) [Dataset]. CMIP5. Retrieved from https://esgf-node.llnl.gov/projects/cmip6/

Coumou, D., Di Capua, G., Vavrus, S., Wang, L., & Wang, S. (2018). The influence of arctic amplification on mid-latitude summer circulation. *Nature Communications*, *9*(1), 2959. https://doi.org/10.1038/s41467-018-05256-8

Dai, Y., Feldstein, S. B., Tan, B., & Lee, S. (2017). Formation mechanisms of the Pacific–North American teleconnection with and without its canonical tropical convection pattern. *Journal of Climate*, *30*(9), 3139–3155. https://doi.org/10.1175/JCLI-D-16-0411.1

Ding, S., Chen, W., Graf, H.-F., Guo, Y., & Nath, D. (2018). Distinct winter patterns of tropical pacific convection anomaly and the associated extratropical wave trains in the northern hemisphere. *Climate Dynamics*, *51*(5), 2003–2022. https://doi.org/10.1007/s00382-017-3995-0

Duan, A., Sun, R., & He, J. (2017). Impact of surface sensible heating over the Tibetan plateau on the western pacific subtropical high: A land–air–sea interaction perspective. *Advances in Atmospheric Sciences*, *34*(2), 157–168. https://doi.org/10.1007/s00376-016-6008-z

Emanuel, K. A., David Neelin, J., & Bretherton, C. S. (1994). On large-scale circulations in convecting atmospheres. *Quarterly Journal of the Royal Meteorological Society*, *120*(519), 1111–1143. https://doi.org/10.1002/qj.49712051902

Fereday, D. R., Chadwick, R., Knight, J. R., & Scaife, A. A. (2020). Tropical rainfall linked to stronger future ENSO-NAO teleconnection in CMIP5 models. *Geophysical Research Letters*, *47*(22), e2020GL088664. https://doi.org/10.1029/2020GL088664

Franzke, C., Feldstein, S. B., & Lee, S. (2011). Synoptic analysis of the Pacific–North American teleconnection pattern. *Quarterly Journal of the Royal Meteorological Society*, *137*(655), 329–346. https://doi.org/10.1002/qj.768

Gan, B., & Wu, L. (2012). Modulation of atmospheric response to North Pacific SST anomalies under global warming: A statistical assessment. *Journal of Climate*, *25*(19), 6554–6566. https://doi.org/10.1175/JCLI-D-11-00493.1

Gill, A. E. (1980). Some simple solutions for heat-induced tropical circulation. *Quarterly Journal of the Royal Meteorological Society*, *106*(449), 447–462. https://doi.org/10.1002/qj.49710644905

Hagos, S., Zhang, C., Tao, W.-K., Lang, S., Takayabu, Y. N., Shige, S., et al. (2010). Estimates of tropical diabatic heating profiles: Commonalities and uncertainties. *Journal of Climate*, *23*(3), 542–558. https://doi.org/10.1175/2009JCLI3025.1

He, C., & Zhou, T. (2014). The two interannual variability modes of the western north pacific subtropical high simulated by 28 CMIP5–AMIP models. *Climate Dynamics*, *43*(9), 2455–2469. https://doi.org/10.1007/s00382-014-2068-x

He, C., & Zhou, T. (2015). Responses of the western north pacific subtropical high to global warming under RCP4.5 and RCP8.5 scenarios projected by 33 CMIP5 models: The dominance of tropical Indian Ocean–tropical western pacific SST gradient. *Journal of Climate*, *28*(1), 365–380. https://doi.org/10.1175/JCLI-D-13-00494.1

He, J., & Soden, B. J. (2015). Anthropogenic weakening of the tropical circulation: The relative roles of direct CO_2 forcing and sea surface temperature change. *Journal of Climate*, *28*(22), 8728–8742. https://doi.org/10.1175/JCLI-D-15-0205.1

He, J., Soden, B. J., & Kirtman, B. (2014). The robustness of the atmospheric circulation and precipitation response to future anthropogenic surface warming. *Geophysical Research Letters*, *41*(7), 2614–2622. https://doi.org/10.1002/2014GL059435

Held, I. M., Ting, M., & Wang, H. (2002). Northern winter stationary waves: Theory and modeling. *Journal of Climate*, *15*(16), 2125–2144. https://doi.org/10.1175/1520-0442(2002)015⟨2125:NWSWTA⟩2.0.CO;2

Hoskins, B. J., James, I. N., & White, G. H. (1983). The shape, propagation and mean-flow interaction of large-scale weather systems. *Journal of the Atmospheric Sciences*, *40*(7), 1595–1612. https://doi.org/10.1175/1520-0469(1983)040⟨1595:TSPAMF⟩2.0.CO;2

Huang, D., Liu, A., Zheng, Y., & Zhu, J. (2022). Inter-model spread of the simulated East Asian summer monsoon rainfall and the associated atmospheric circulations from the CMIP6 models. *Journal of Geophysical Research: Atmospheres*, *127*(20), e2022JD037371. https://doi.org/10.1029/2022JD037371

Huang, P., Xie, S.-P., Hu, K., Huang, G., & Huang, R. (2013). Patterns of the seasonal response of tropical rainfall to global warming. *Nature Geoscience*, *6*(5), 357–361. https://doi.org/10.1038/ngeo1792

Hurrell, J. W., Holland, M. M., Gent, P. R., Ghan, S., Kay, J. E., Kushner, P. J., et al. (2013). The community Earth system model: A framework for collaborative research. *Bulletin of the American Meteorological Society*, *94*(9), 1339–1360. https://doi.org/10.1175/BAMS-D-12-00121.1

Kay, J. E., Deser, C., Phillips, A., Mai, A., Hannay, C., Strand, G., et al. (2015). The community Earth system model (CESM) large ensemble project: A community resource for studying climate change in the presence of internal climate variability. *Bulletin of the American Meteorological Society*, *96*(8), 1333–1349. https://doi.org/10.1175/BAMS-D-13-00255.1

Kosaka, Y., Xie, S.-P., Lau, N.-C., & Vecchi, G. A. (2013). Origin of seasonal predictability for summer climate over the northwestern Pacific. *Proceedings of the National Academy of Sciences*, *110*(19), 7574–7579. https://doi.org/10.1073/pnas.1215582110

Levine, X. J., & Boos, W. R. (2019). Sensitivity of subtropical stationary circulations to global warming in climate models: A Baroclinic Rossby gyre theory. *Climate Dynamics*, *52*(7), 4873–4890. https://doi.org/10.1007/s00382-018-4419-5

Levine, X. J., & Boos, W. R. (2017). Land surface albedo bias in climate models and its association with tropical rainfall. *Geophysical Research Letters*, *44*(12), 6363–6372. https://doi.org/10.1002/2017GL072510

Li, W., Li, L., Ting, M., & Liu, Y. (2012). Intensification of northern hemisphere subtropical highs in a warming climate. *Nature Geoscience*, *5*(11), 830–834. https://doi.org/10.1038/ngeo1590

Lindzen, R. S., & Nigam, S. (1987). On the role of sea surface temperature gradients in forcing low-level winds and convergence in the tropics. *Journal of the Atmospheric Sciences*, *44*(17), 2418–2436. https://doi.org/10.1175/1520-0469(1987)044⟨2418:OTROSS⟩2.0.CO;2

Lu, K., He, J., & Simpson, I. (2023). Origins of uncertainty in projections of summer north Pacific subtropical high [Dataset]. Zenodo. https://doi.org/10.5281/zenodo.8327817

Matsuno, T. (1966). Quasi-geostrophic motions in the equatorial area. *Journal of the Meteorological Society of Japan. Ser. II*, *44*(1), 25–43. https://doi.org/10.2151/jmsj1965.44.1{_}25

Mauritsen, T., & Stevens, B. (2015). Missing iris effect as a possible cause of muted hydrological change and high climate sensitivity in models. *Nature Geoscience*, *8*(5), 346–351. https://doi.org/10.1038/ngeo2414

Mestas-Nuñez, A. M. (2000). Orthogonality properties of rotated empirical modes. *International Journal of Climatology*, *20*(12), 1509–1516. https://doi.org/10.1002/1097-0088(200010)20:12⟨1509::AID-JOC553⟩3.0.CO;2-Q

O'Neill, B. C., Tebaldi, C., van Vuuren, D. P., Eyring, V., Friedlingstein, P., Hurtt, G., et al. (2016). The scenario model intercomparison project (scenariomip) for CMIP6. *Geoscientific Model Development*, *9*(9), 3461–3482. https://doi.org/10.5194/gmd-9-3461-2016

Park, M., & Lee, S. (2021). Is the stationary wave bias in CMIP5 simulations driven by latent heating biases? *Geophysical Research Letters*, *48*(4), e2020GL091678. https://doi.org/10.1029/2020GL091678

Portal, A., Pasquero, C., D'Andrea, F., Davini, P., Hamouda, M. E., & Rivière, G. (2022). Influence of reduced winter land–sea contrast on the midlatitude atmospheric circulation. *Journal of Climate*, *35*(19), 2637–2651. https://doi.org/10.1175/JCLI-D-21-0941.1

Rodwell, M. J., & Hoskins, B. J. (2001). Subtropical anticyclones and summer monsoons. *Journal of Climate*, *14*(15), 3192–3211. https://doi.org/10.1175/1520-0442(2001)014⟨3192:SAASM⟩2.0.CO;2

Seager, R., Osborn, T. J., Kushnir, Y., Simpson, I. R., Nakamura, J., & Liu, H. (2019). Climate variability and change of Mediterranean-type climates. *Journal of Climate*, *32*(10), 2887–2915. https://doi.org/10.1175/JCLI-D-18-0472.1

Shaw, T. A., & Voigt, A. (2015). Tug of war on summertime circulation between radiative forcing and sea surface warming. *Nature Geoscience*, *8*(7), 560–566. https://doi.org/10.1038/ngeo2449

Sigmond, M., Kushner, P. J., & Scinocca, J. F. (2007). Discriminating robust and non-robust atmospheric circulation responses to global warming. *Journal of Geophysical Research*, *112*(D20). https://doi.org/10.1029/2006JD008270

Su, H., Jiang, J. H., Neelin, J. D., Shen, T. J., Zhai, C., Yue, Q., et al. (2017). Tightening of tropical ascent and high clouds key to precipitation change in a warmer climate. *Nature Communications*, *8*(1), 15771. https://doi.org/10.1038/ncomms15771

Sui, C.-H., Chung, P.-H., & Li, T. (2007). Interannual and interdecadal variability of the summertime western north pacific subtropical high. *Geophysical Research Letters*, *34*(11), L11701. https://doi.org/10.1029/2006GL029204

Takaya, K., & Nakamura, H. (1997). A formulation of a wave-activity flux for stationary Rossby waves on a zonally varying basic flow. *Geophysical Research Letters*, *24*(23), 2985–2988. https://doi.org/10.1029/97GL03094

Taylor, K. E., Stouffer, R. J., & Meehl, G. A. (2012). An overview of CMIP5 and the experiment design. *Bulletin of the American Meteorological Society*, *93*(4), 485–498. https://doi.org/10.1175/BAMS-D-11-00094.1

Ting, M., Wang, H., & Yu, L. (2001). Nonlinear stationary wave maintenance and seasonal cycle in the GFDL R30 GCM. *Journal of the Atmospheric Sciences*, *58*(16), 2331–2354. https://doi.org/10.1175/1520-0469(2001)058⟨2331:NSWMAS⟩2.0.CO;2

Ting, M., & Yu, L. (1998). Steady response to tropical heating in wavy linear and nonlinear baroclinic models. *Journal of the Atmospheric Sciences*, *55*(24), 3565–3582. https://doi.org/10.1175/1520-0469(1998)055⟨3565:SRTTHI⟩2.0.CO;2

Wang, B., Xiang, B., & Lee, J.-Y. (2013). Subtropical high predictability establishes a promising way for monsoon and tropical storm predictions. *Proceedings of the National Academy of Sciences*, *110*(8), 2718–2722. https://doi.org/10.1073/pnas.1214626110

Wang, X., Xie, S.-P., Guan, Z., & Wang, M. (2021). A common base mode of Asian summer monsoon variability across timescales. *Journal of Climate*, *34*(18), 7359–7371. https://doi.org/10.1175/JCLI-D-20-0856.1

Wang, Y., Wu, B., & Zhou, T. (2022). Maintenance of western north pacific anomalous anticyclone in boreal summer by wind-induced moist enthalpy advection mechanism. *Journal of Climate*, *35*(14), 4499–4511. https://doi.org/10.1175/JCLI-D-21-0708.1

Weare, B. C., Navato, A. R., & Newell, R. E. (1976). Empirical orthogonal analysis of pacific sea surface temperatures. *Journal of Physical Oceanography*, *6*(5), 671–678. https://doi.org/10.1175/1520-0485(1976)006⟨0671:EOAOPS⟩2.0.CO;2

Webb, M. J., Andrews, T., Bodas-Salcedo, A., Bony, S., Bretherton, C. S., Chadwick, R., et al. (2017). The cloud feedback model intercomparison project (CFMIP) contribution to CMIP6. *Geoscientific Model Development*, *10*(1), 359–384. https://doi.org/10.5194/gmd-10-359-2017

Wills, R. C. J., White, R. H., & Levine, X. J. (2019). Northern hemisphere stationary waves in a changing climate. *Current Climate Change Reports*, *5*(4), 372–389. https://doi.org/10.1007/s40641-019-00147-6

Wu, B., Zhou, T., & Li, T. (2017). Atmospheric dynamic and thermodynamic processes driving the western north pacific anomalous anticyclone during El Niño. Part I: Maintenance mechanisms. *Journal of Climate*, *30*(23), 9621–9635. https://doi.org/10.1175/JCLI-D-16-0489.1

Xie, S.-P., Deser, C., Vecchi, G. A., Ma, J., Teng, H., & Wittenberg, A. T. (2010a). Global warming pattern formation: Sea surface temperature and rainfall. *Journal of Climate*, *23*(4), 966–986. https://doi.org/10.1175/2009JCLI3329.1

Xie, S.-P., Deser, C., Vecchi, G. A., Ma, J., Teng, H., & Wittenberg, A. T. (2010b). Global warming pattern formation: Sea surface temperature and rainfall. *Journal of Climate*, *23*(4), 966–986. https://doi.org/10.1175/2009JCLI3329.1

Xie, S.-P., Hu, K., Hafner, J., Tokinaga, H., Du, Y., Huang, G., & Sampe, T. (2009). Indian ocean capacitor effect on indo–western pacific climate during the summer following El Niño. *Journal of Climate*, *22*(3), 730–747. https://doi.org/10.1175/2008JCLI2544.1

Zhou, S., Huang, P., Huang, G., & Hu, K. (2019). Leading source and constraint on the systematic spread of the changes in east Asian and western north pacific summer monsoon. *Environmental Research Letters*, *14*(12), 124059. https://doi.org/10.1088/1748-9326/ab547c

Zhou, W., & Xie, S.-P. (2017). Intermodel spread of the double-ITCZ bias in coupled GCMS tied to land surface temperature in AMIP GCMS. *Geophysical Research Letters*, *44*(15), 7975–7984. https://doi.org/10.1002/2017GL074377